



Effects of the Support-Crystal Size on the Catalytic Performance of RuO₂/TiO₂ in the Deacon Process

Xue Wang¹ · Yupei Liu¹ · Chunhui Xu¹ · Xinqing Lu^{1,2} · Rui Ma^{1,2} · Yanghe Fu^{1,2} · Shuhua Wang³ · Weidong Zhu^{1,2,3}

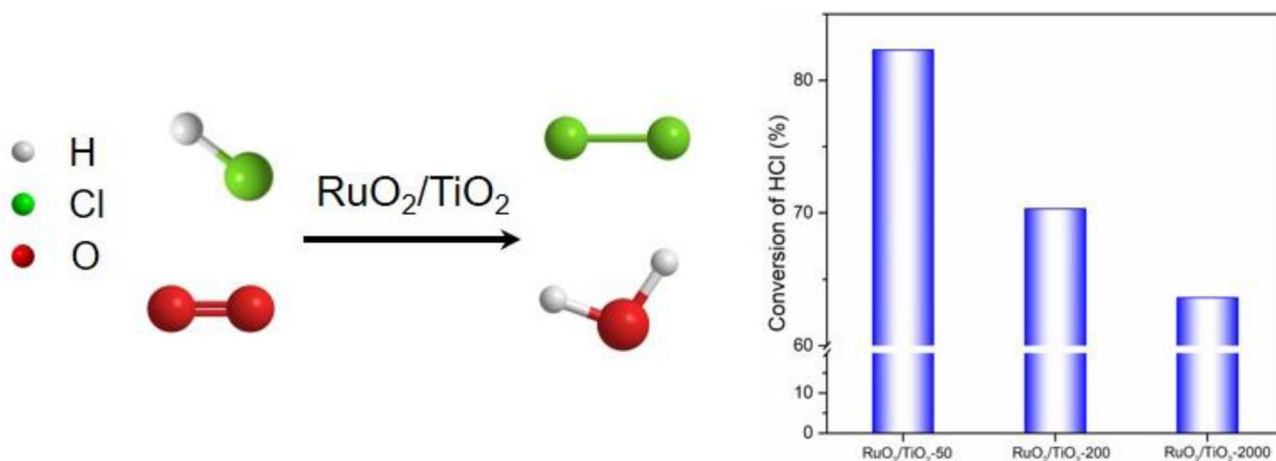
Received: 13 August 2020 / Accepted: 3 December 2020

© The Author(s), under exclusive licence to Springer Science+Business Media, LLC part of Springer Nature 2021

Abstract

RuO₂/TiO₂ catalysts with different TiO₂ crystal sizes were prepared via a dry impregnation method, and these prepared catalysts were applied in the oxidation of HCl. The results show that decreasing the support-crystal size is an effective method to enhance the dispersion of RuO₂ on TiO₂, which is helpful to increase the catalytic activity significantly.

Graphic Abstract



Keywords TiO₂ · Support-size effect · RuO₂ · Dispersion · Deacon process

Supplementary information The online version of this article (<https://doi.org/10.1007/s10562-020-03493-5>) contains supplementary material, which is available to authorized users.

✉ Xinqing Lu
xinqinglu@zjnu.cn

✉ Weidong Zhu
weidongzhu@zjnu.cn

¹ Zhejiang Engineering Laboratory for Green Syntheses and Applications of Fluorine-Containing Specialty Chemicals, Institute of Advanced Fluorine-Containing Materials, Zhejiang Normal University, Jinhua 321004, People's Republic of China

² Key Laboratory of the Ministry of Education for Advanced Catalysis Materials, Institute of Physical Chemistry, Zhejiang Normal University, Jinhua 321004, People's Republic of China

³ National Engineering Technology Research Center of Fluoro-Materials, Zhejiang Juhua Technology Center Co., Ltd, Quzhou 324004, People's Republic of China

1 Introduction

Chlorine is widely used as a reactive intermediate for manufacturing industrial and consumer products, especially polyurethane and polycarbonate. However, approximately 50% of the Cl_2 produced worldwide ends up as HCl or chloride salts [1]. The most representative example is the production of toluene diisocyanate (TDI), in which 4 mol of HCl are produced for each mole of TDI production while the produced HCl is environmentally undesirable and has a limited market. Consequently, it is attractive to find efficient methods for converting the by-product HCl in waste streams back into the reactive intermediate Cl_2 .

The heterogeneously catalyzed gas-phase oxidation of HCl by molecular oxygen to H_2O and Cl_2 , the so-called Deacon process, is a sustainable route to meet the world's growing demand for Cl_2 and to recycle the by-product HCl in the chlorine-related chemical industry [2, 3], showing a lower energy consumption than that by an electro-catalyzed chlorine evolution reaction. In the Deacon process, it has been repeatedly demonstrated that supported RuO_2 catalysts are effective because of their high activities at low temperatures and resistance to bulk chlorination [4]. Both TiO_2 (rutile) and SnO_2 (cassiterite) have been identified as the best supports for preparing supported RuO_2 Deacon catalysts, because RuO_2 is deposited in the form of epitaxially grown structures as a result of lattice matching, leading to an enhanced dispersion and stabilization of the active phase, which is quite different from other supports, such as SiO_2 , Al_2O_3 , and TiO_2 with an anatase-type structure [5–10]. Additionally, rutile- TiO_2 supported RuO_2 catalysts are also highly active in many other important reactions, such as photocatalytic water splitting [11], trichloroethylene oxidation [12], CO oxidation [13], dehydrogenation of NH_3 [14] and CH_3OH [15], and electrocatalysis [3]. Furthermore, a transient mechanistic study has demonstrated that the surface $\text{RuO}_{2-x}\text{Cl}_x$ oxychloride formed via the partial chlorination of the surface Ru atoms (coordinatively unsaturated and bridge sites) is the active phase, indicating that the catalytic performance of supported RuO_2 catalysts is closely related to the amount of the surface Ru atoms [16–18]. Hence, it is attractive to increase the percentage of the surface Ru atoms by increasing the dispersion of RuO_2 on the supports.

Strengthening the active phase-support interactions by optimizing the synthesis parameters during the catalyst preparation has been demonstrated as an effective way to increase the dispersion of RuO_2 on the supports [8, 19–21]. Pérez-Ramírez et al. [21] have found that depositing colloiddally prepared Ru nanoparticles on a rutile carrier results in catalysts attaining a higher activity in the Deacon process, compared to the catalyst with the

same Ru content prepared by a conventional impregnation method. Additionally, it is expected that the dispersion of RuO_2 might be enhanced by decreasing the support-crystal size, because the smaller the support-crystal size, the higher the specific surface area for carrying the active species. However, the effects of the support-crystal size on the catalytic properties of the Deacon catalyst $\text{RuO}_2/\text{TiO}_2$ have not been systematically investigated yet.

In this work, $\text{RuO}_2/\text{TiO}_2$ catalysts with different support-crystal sizes were prepared and characterized with various techniques in detail. These prepared catalysts were then evaluated in the Deacon process and the effects of the support-crystal size on the catalytic properties of the resultant $\text{RuO}_2/\text{TiO}_2$ in the HCl oxidation were systematically investigated. The results show that the decrease of the support-crystal size can be an effective method to enhance the dispersion of RuO_2 on TiO_2 , leading to a significant increase in the catalytic activity.

2 Experimental

2.1 Catalyst Preparation

Based on the recipe and synthesis procedure reported in the literature [22], the rutile-type TiO_2 support with a crystal size of *ca.* 2000 nm was prepared as follows, 0.6 g of TiCl_4 was dissolved in 100 mL of HCl aqueous solution (3.5 M) with stirring in an ice-water bath, followed by adding 0.07 g of NaF. The obtained reaction mixture was then hydrothermally crystallized at 493 K for 12 h and cooled to room temperature. The product was washed with distilled water and then dried at 373 K overnight. Finally, the dried sample was calcined in static air at 773 K for 5 h with a heating rate of 5 K min^{-1} , and the calcined sample was named TiO_2 -2000.

For comparison, two commercially available rutile-type TiO_2 samples with average crystal sizes of *ca.* 200 and 50 nm in diameter, purchased from Shanghai Xushuo Biotechnology Co., Ltd., were calcined under the same conditions as those for the synthesized one to ensure their rutile-type structures, and these calcined samples were named TiO_2 -200 and TiO_2 -50, respectively.

The $\text{RuO}_2/\text{TiO}_2$ catalysts (nominal 2.0 wt% Ru with different support-crystal sizes) were prepared by a dry impregnation method as follows, 1.0 g of TiO_2 support was impregnated with 0.1 mL of RuCl_3 aqueous solution (0.1 g mL^{-1}) at room temperature for 6 h. In addition, the $\text{RuO}_2/\text{TiO}_2$ -50 catalysts with nominal 1.5 and 2.5 wt% Ru loadings were also prepared by the dry impregnation method as follows: 1.0 g of TiO_2 -50 was impregnated with 0.1 mL of RuCl_3 aqueous solution (a RuCl_3 concentration of 0.075 or 0.125 g mL^{-1}) at room temperature for 6 h. Then the above-obtained slurry was dried at 343 K for 12 h and calcined in

static air at 523 K for 16 h with a heating rate of 5 K min⁻¹. If not mentioned, the nominal Ru loading in the RuO₂/TiO₂ catalysts refers to 2.0 wt%.

2.2 Characterization

The powder X-ray diffractometry (XRD) patterns were recorded on a Philips PW3040/60 powder diffractometer using Ni-filtered Cu K α radiation ($\lambda = 0.1541$ nm) in the 2θ range of 20°–80° with a scanning rate of 2° min⁻¹. The morphologies and sizes of the support crystals were determined by scanning electron microscopy (SEM) on a ZEISS GeminiSEM 300 microscope. The RuO₂ particle sizes on the supports were determined by TEM on a JEOL JEM-2100 microscope at 200 kV after the samples were deposited onto a holey carbon foil supported on a copper grid. The textural properties of the samples were determined by N₂ adsorption–desorption at 77 K using a Micromeritics ASAP 2020 instrument after the samples were degassed under a vacuum at 523 K for 6 h. The Raman spectra were collected on a Renishaw In-Via Reflex Raman microscope equipped with Renishaw diode laser 532 nm at a resolution of 3 cm⁻¹. The X-ray photoelectron spectra (XPS) were obtained with a Thermo Scientific ESCALAB250xi instrument using monochromatic Al K α radiation and operating at a constant power of 200 W. The reduction temperature of metal oxides was determined by H₂-TPR (temperature-programmed reduction) on a Micromeritics AutoChem II 2920 instrument equipped with a thermal conductivity detector (TCD). Typically, 0.1 g of the sample was pretreated in flowing helium with a rate of 30 mL min⁻¹ at 473 K for 1 h. The H₂-TPR profile was then recorded from 323 to 1073 K with a heating rate of 10 K min⁻¹ in 5 vol.% H₂ in Ar with a total flow rate of 30 mL min⁻¹.

2.3 Catalytic Oxidation of HCl

The catalytic oxidation of HCl was carried out in a fixed-bed reactor (8 mm inner diameter) at atmosphere pressure. The catalyst was pressed at 8.0 MPa and then crushed into particles ranging from 0.18 to 0.25 mm in diameter. The reactor was loaded with 0.2 g of the pellet catalyst. After the reactor temperature was heated up to 623 K in flowing N₂ with a rate of 30 mL min⁻¹, the N₂ flow was switched off and a mixture of HCl and O₂ was introduced into the reactor. In the current investigation, the weight hourly space velocity (WHSV) of HCl was maintained at 39.1 h⁻¹, and the molar ratio of O₂ to HCl varied from 2:8 to 4:8. The same amount of the pellet support as that of the catalyst loaded in the reactor was used for a blank experiment to check whether the support was also active in the oxidation. The reaction effluent was absorbed by an excessive KI solution and the absorbed solution was analyzed by iodometry and acid–base titration

every 15 min to determine the produced Cl₂ and unconverted HCl amounts. Consequently, the chlorine balances were calculated by comparing the total mole of chlorine in the reactant stream with the one in the absorbed solution and the conversion of HCl as a function of time on stream was determined as well.

3 Results and Discussion

3.1 Catalyst Characterization

The morphology and phase purity of the TiO₂ supports used were examined by the SEM and XRD techniques. As shown in Fig. S1, the SEM images indicate that the three different TiO₂ supports have average crystal sizes of *ca.* 50, 200, and 2000 nm, respectively. Fig. S2 shows the XRD patterns of these three TiO₂ supports in comparison with the standard pattern of rutile-type TiO₂ (JCPDS No. 21-1276). All the diffraction peaks in the XRD patterns can be indexed as a pure rutile phase and are fully consistent with the standard ones of rutile TiO₂. Moreover, a significant difference in the intensity of peaks is observed, mainly due to their different crystal sizes. The Brunauer–Emmett–Teller (BET) specific surface area is the total of the internal and external specific surface areas. As shown in Table S1, the external specific surface areas are very closely to the BET ones for the three supports, indicating that all the investigated TiO₂ supports are non-porous. In other words, only the external surfaces of the supports can offer the platform for the loading of RuO₂. In addition, the measured external specific surface area, S_{ext} , of the support decreases with increasing the crystal size significantly.

The TEM experiments were carried out to determine the particle size of the active phase RuO₂ in the three different catalysts. As shown in Fig. 1, with the same nominal Ru loading in the three different catalysts, the mean diameter of RuO₂ particles decreases from *ca.* 2.6 nm in RuO₂/TiO₂-2000 to *ca.* 2.3 nm in RuO₂/TiO₂-200 and *ca.* 2.0 nm in RuO₂/TiO₂-50, implying that the active phase RuO₂ is better dispersed on the surface of the TiO₂ support with a small crystal size. Additionally, it is also observed that the mean diameter of RuO₂ particles in RuO₂/TiO₂-50 increases with increasing the nominal Ru loading (Fig. S3). Hence, both the support TiO₂ crystal size and the Ru loading dominate the particle size of the active phase RuO₂ in the resultant catalyst.

The Raman spectroscopy was employed to investigate the electronic interactions between the active phase RuO₂ and the support TiO₂. As shown in Fig. 2, the characteristic bands of the TiO₂ supports are observed at 143, 234, 441, and 606 cm⁻¹, which can be assigned to B_{1g} , two-photon scattering process, E_g (planar O–O vibration), and A_{1g} (Ti–O

Fig. 1 TEM images of RuO₂/TiO₂-50 (a), RuO₂/TiO₂-200 (b), and RuO₂/TiO₂-2000 (c)

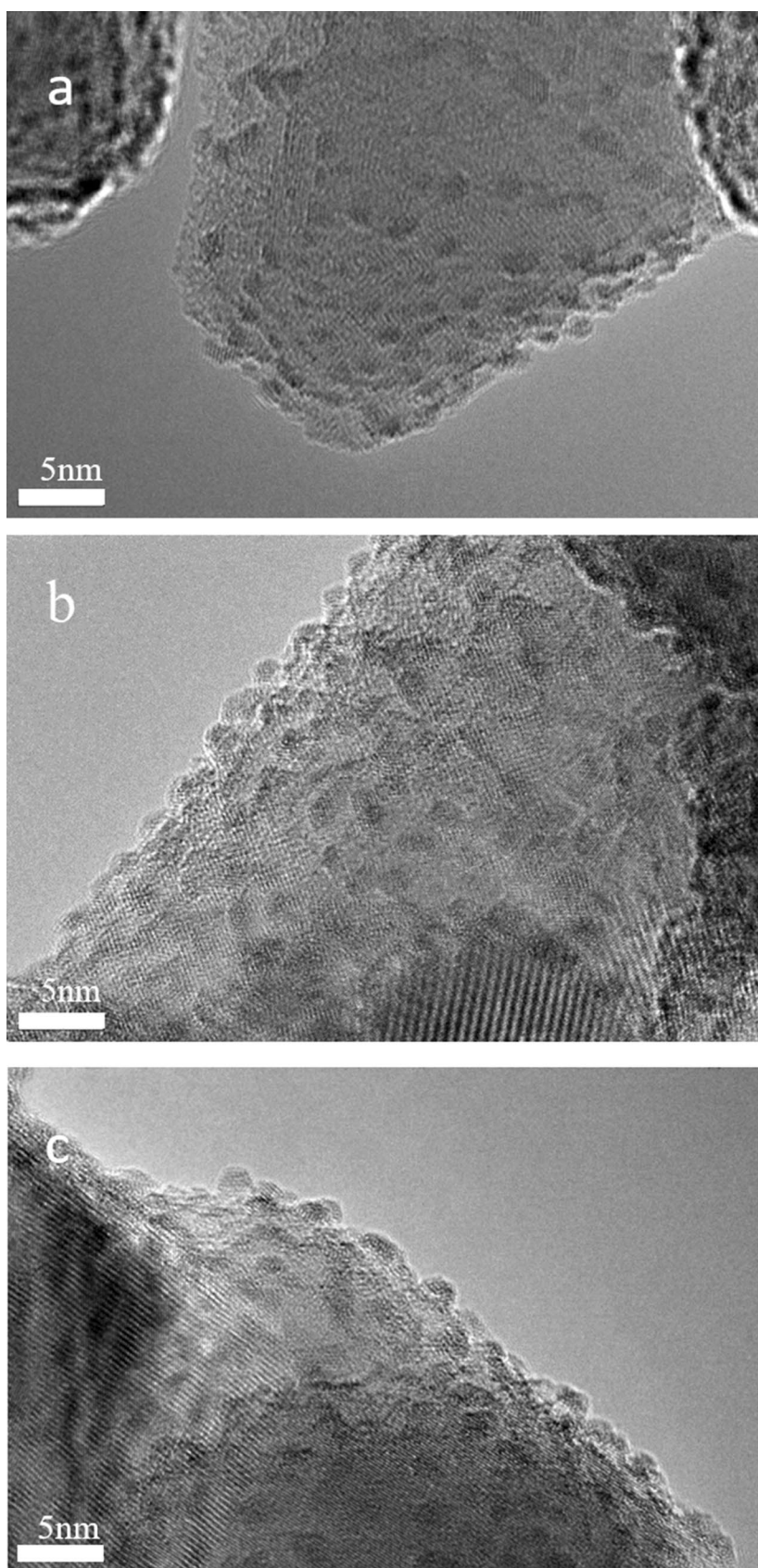
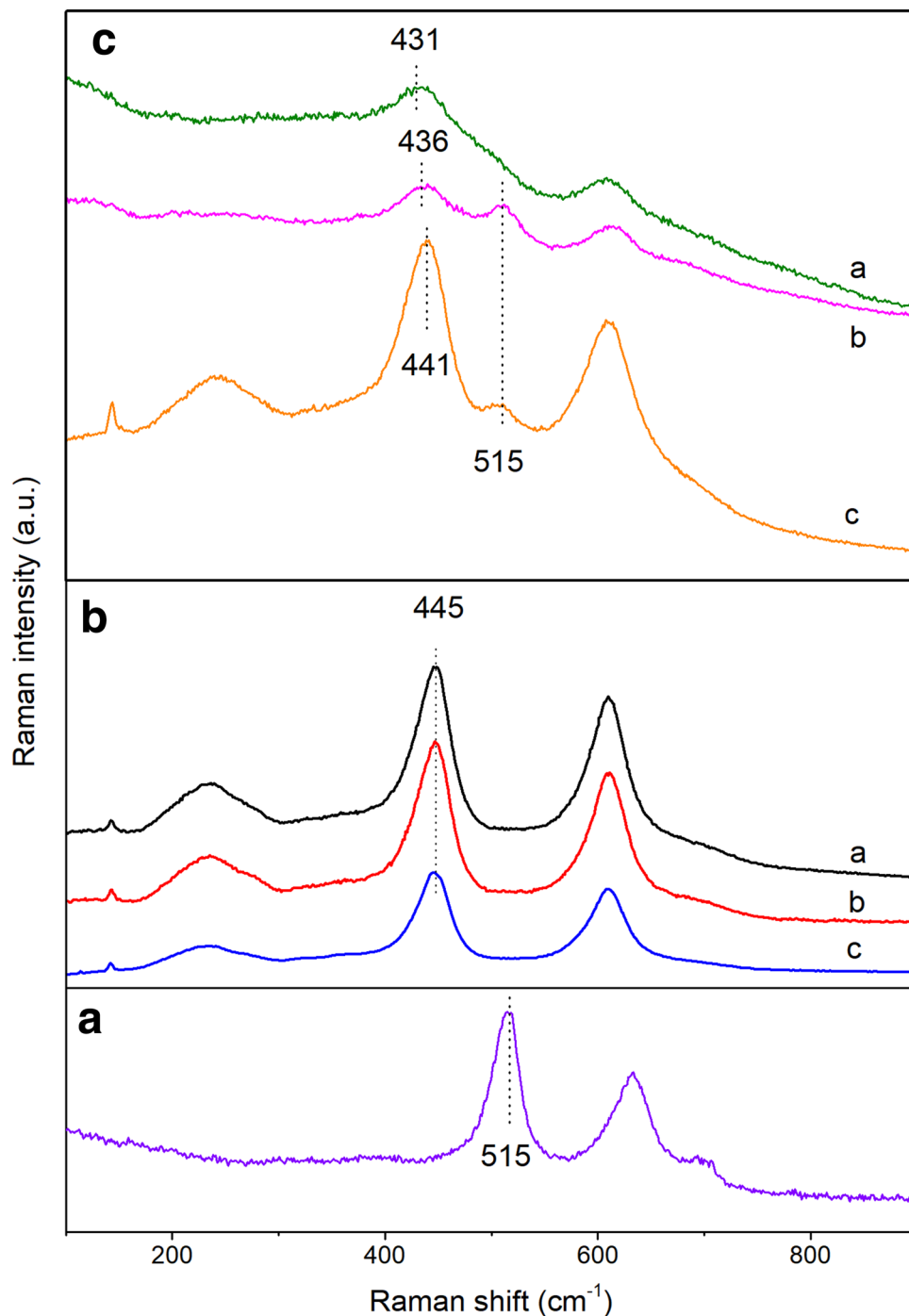


Fig. 2 Raman spectra of rutile-RuO₂ (a), supports TiO₂-x (b), and catalysts RuO₂/TiO₂-x (c). The x represents a TiO₂ crystal size of ca. 50 nm (a), 200 nm (b), and 2000 nm (c), respectively, and the same below



stretch) Raman-active modes, respectively [23–25]. In the case of RuO₂/TiO₂-2000 (Fig. 2c), the shift of the E_g peak to a lower wavenumber suggests that the electron transfer from RuO₂ to TiO₂ results from the formation of Ru–O–Ti linkage [13]. More interestingly, it can be seen that the Raman shift from TiO₂ to RuO₂/TiO₂ increases with decreasing the support-crystal size, indicating that more Ru–O–Ti linkages are formed. In other words, the active phase RuO₂ is better dispersed on the surface of a relatively smaller crystal-size TiO₂

support. In addition, RuO₂/TiO₂-2000 shows a new band emerged at 515 cm⁻¹ assigned to the E_g mode of rutile-type RuO₂ crystals, implying that the RuO₂ is poorly dispersed and inclines to aggregate to form microcrystallites. Fortunately, the band at 515 cm⁻¹ is absent for RuO₂/TiO₂-50, further demonstrating that the TiO₂ support with the smallest crystal size will be the best for the dispersion of RuO₂.

The XPS technique was also employed to investigate the state of the Ru species in the catalysts. It is well known

that XPS is a surface-sensitive technique for the analysis of elements and their oxidation states, and the binding energy (BE) is closely related to the estimated charges on the central atoms. As shown in Fig. 3, the Ru 3d_{5/2} bands at binding energies of around 282 and 281 eV are assigned to Ru⁴⁺ and Ru³⁺, respectively [26]. The percentage of Ru⁴⁺ increases from 53.7% for RuO₂/TiO₂-2000 to 70.2% and 100% for RuO₂/TiO₂-200 and RuO₂/TiO₂-50, respectively, indicating that more electron transfer from RuO₂ to TiO₂ results from the formation of more Ru–O–Ti linkages in the catalysts with the relatively smaller crystal-size support.

The H₂-TPR analysis was carried out to study the interactions between the active phase RuO₂ and the support TiO₂. The H₂-TPR profiles of the TiO₂ supports and the corresponding RuO₂/TiO₂ catalysts are shown in Figs. 4 and S4, respectively. In a temperature range from 323 to 1073 K, all the peaks in the catalysts are assigned to the reduction of the active phase RuO₂ rather than that of the support TiO₂, because no reduction peak is observed in all the TiO₂ supports at the conditions investigated. It is reported that the reduction temperature of Ru–O–Ti is higher than that of Ru–O–Ru [27]. In this study, it is noteworthy that the reduction temperature of RuO₂ increases from 397 K for RuO₂/TiO₂-2000 to 498 K for RuO₂/TiO₂-50. This could be concluded that more Ru–O–Ti species are formed in RuO₂/TiO₂-50, which is in good accordance with the observation from the Raman spectra.

In summary, all of the TEM, Raman, XPS, and H₂-TPR characterization results show that the support with a smaller crystal size will be helpful to form more Ru–O–Ti species, leading to a better dispersion of RuO₂ on the support surface.

3.2 Catalytic Oxidation of HCl

The catalytic activities of the TiO₂ supports and the RuO₂/TiO₂ catalysts were investigated in the gas-phase oxidation of HCl. The supports do not show any activity, as expected. It has been demonstrated that the surface RuO_{2-x}Cl_x oxychloride formed by the partial chlorination of the surface Ru atoms (coordinatively unsaturated and bridge sites) is the active phase. Therefore, the catalytic activity of RuO₂/TiO₂ is closely related to the amount of the surface Ru atoms [16]. As shown in Fig. 5, RuO₂/TiO₂ catalysts with the different TiO₂ crystal sizes have almost identical TOF values in the catalytic reaction. However, the conversion of HCl increases in the order of RuO₂/TiO₂-2000 < RuO₂/TiO₂-200 < RuO₂/TiO₂-50, which could be ascribed to the effects of the support-crystal size. TiO₂ with a smaller crystal size, possessing a larger external surface area, will promote the formation of the more surface RuO₂, resulting in the enhanced catalytic activity in the oxidation of HCl. It is also worthy of note

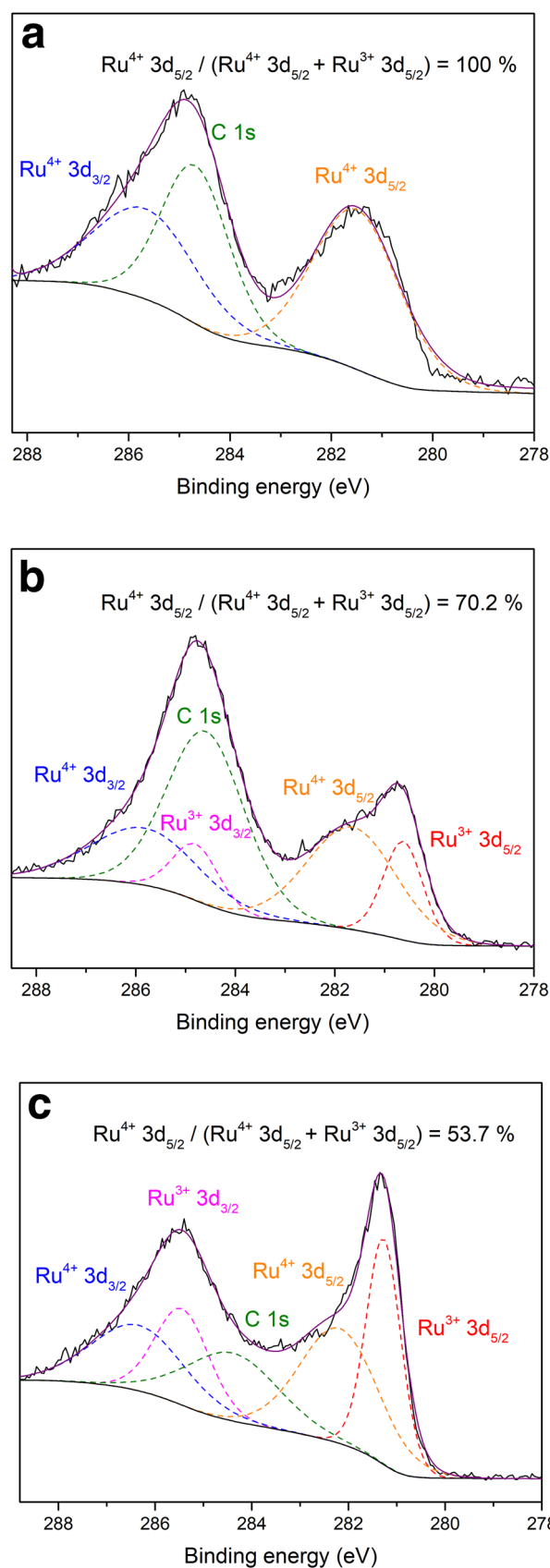
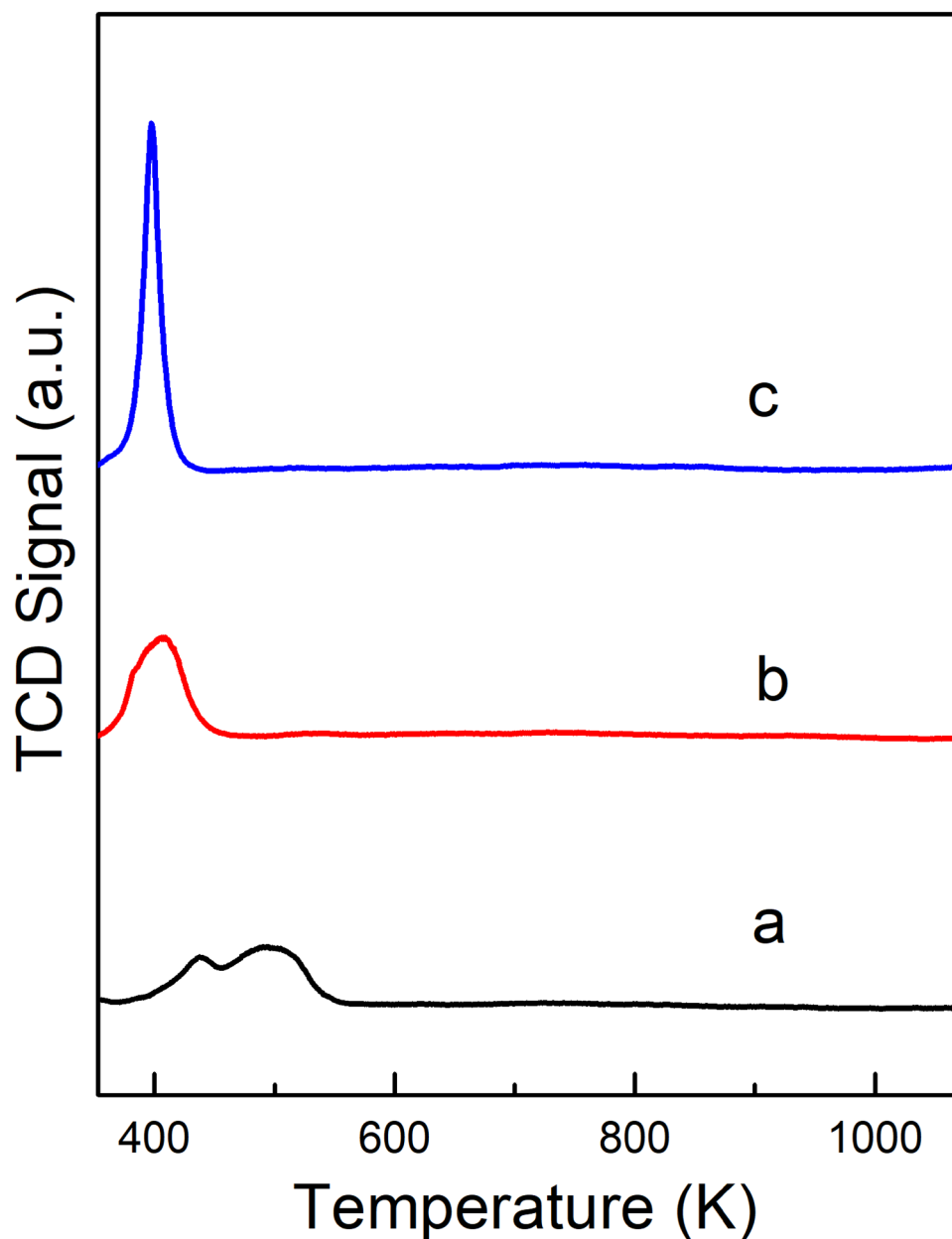


Fig. 3 Ru 3d XPS spectra of RuO₂/TiO₂-50 (a), RuO₂/TiO₂-200 (b), and RuO₂/TiO₂-2000 (c)

Fig. 4 H₂-TPR profiles of RuO₂/TiO₂ catalysts

that the conversion of HCl over RuO₂/TiO₂-50 is 82.3%, close to its equilibrium conversion (87.0%) at the applied reaction conditions. Moreover, the molar ratio of O₂ to HCl plays a critical role in the reaction (Fig. 6), i.e., a high O₂ partial pressure is beneficial for Cl₂ production. Furthermore, the conversion of HCl over the RuO₂/TiO₂-50 catalyst increases with increasing Ru loading while these catalysts have almost identical TOF values (Fig. S5). A similar observation has also been found in the hydrogenation of cyclohexene over the supported platinum catalysts [28, 29].

4 Conclusions

The RuO₂/TiO₂ catalysts with different support-crystal sizes were prepared via the impregnation method and these prepared catalysts were used in the HCl oxidation to Cl₂. The results show that the dispersion of RuO₂ on the surface of TiO₂ with a rutile structure can be effectively controlled by adjusting the support-crystal size. TiO₂ with a smaller crystal size possesses a larger geometric surface area for the loading of RuO₂ and enhances the formation of more Ru–O–Ti species, resulting in a better dispersion of RuO₂

Fig. 5 Comparative results on the oxidation of HCl over different $\text{RuO}_2/\text{TiO}_2$ catalysts. Reaction conditions: WHSV (HCl) = 39.1 h^{-1} , molar ratio of O_2 to HCl = 4:8, and reaction temperature = 623 K

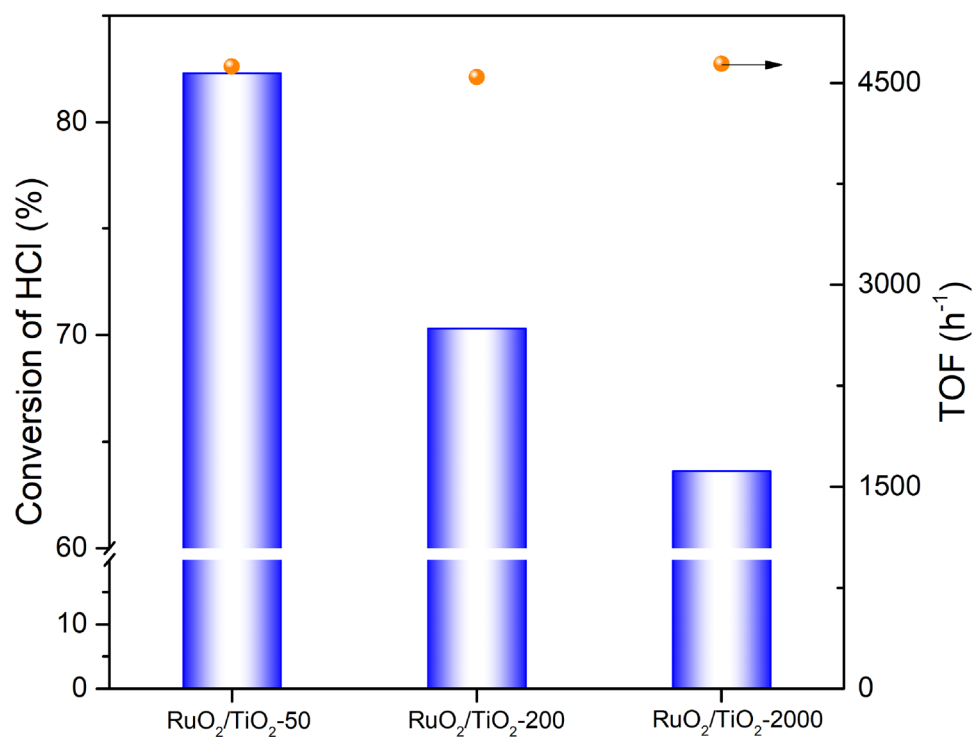
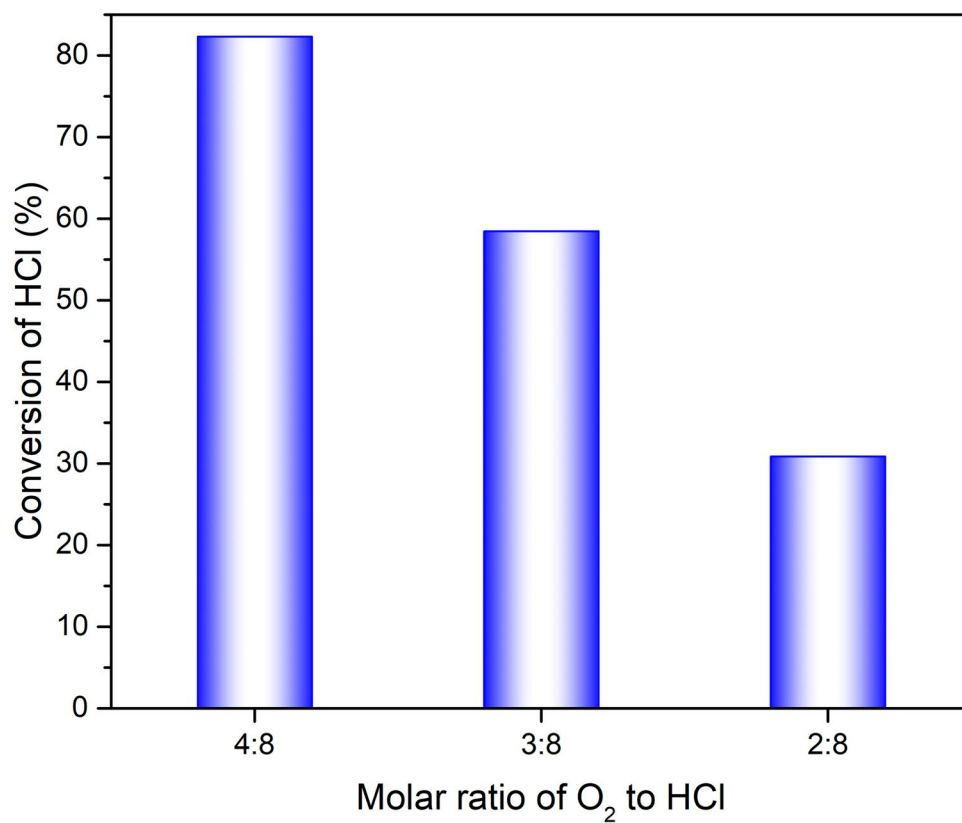


Fig. 6 Effects of the molar ratio of O_2 to HCl on the oxidation of HCl over $\text{RuO}_2/\text{TiO}_2$ -50. Reaction conditions: WHSV (HCl) = 39.1 h^{-1} and reaction temperature = 623 K



on the surface of the support and a higher catalytic activity in the oxidation of HCl. The current work could stimulate fundamental research and industrial applications of highly active Deacon catalysts.

Acknowledgements The authors gratefully acknowledge financial support from Zhejiang Provincial Key R&D Project (2019C03118) and Zhejiang Provincial Natural Science Foundation (Q20B030021).

References

- Motupally S, Mah DT, Freire FJ, Weidner JW (1998) *Electrochem Soc Interface* 7:32
- Pérez-Ramírez J, Mondelli C, Schmidt T, Schlüter OFK, Wolf A, Mleczko L, Dreier T (2011) *Energy Environ Sci* 4:4786
- Over H (2012) *Chem Rev* 112:3356
- Over H, Schomäcker R (2013) *ACS Catal* 3:1034
- Hibi T, Nishida H, Abekawa H (1999) US Patent 5871707.
- Iwanaga K, Seki K, Hibi T, Issoh K, Suzuta T, Nakada M, Mori Y, Abe T (2004) *Sumitomo Kagaku* 2004:1
- Seki K (2010) *Catal Surv Asia* 14:168
- Mondelli C, Amrute AP, Krumeich F, Schmidt T, Pérez-Ramírez J (2011) *ChemCatChem* 3:657
- Teschner D, Farra R, Yao L, Schlögl R, Soerijanto H, Schomäcker R, Schmidt T, Szentmiklósi L, Amrute AP, Mondelli C, Pérez-Ramírez J (2012) *J Catal* 285:273
- Wang D, Huang J, Liu F, Xu X, Fang X, Liu J, Xie Y, Wang X (2020) *Catal Today* 339:220
- Gu Q, Gao Z, Yu S, Xue C (2016) *Adv Mater Interfaces* 3:1500631
- Wang J, Liu X, Zeng J, Zhu T (2016) *Catal Commun* 76:13
- Li H, Zha S, Zhao Z-J, Tian H, Chen S, Gong Z, Cai W, Wang Y, Cui Y, Zeng L, Mu R, Gong J (2018) *ACS Catal* 8:5526
- Nagaoka K, Eboshi T, Takeishi Y, Tasaki R, Honda K, Imamura K, Sato K (2017) *Sci Adv* 3:e1602747
- Zarei M, Davarpanah A, Mokhtarian N, Farahbod F (2020) *Energy Sources Part A* 42:89
- Hevia MAG, Amrute AP, Schmidt T, Pérez-Ramírez J (2010) *J Catal* 276:141
- Zweidinger S, Crihan D, Knapp M, Hofmann JP, Seitsonen AP, Weststrate CJ, Lundgren E, Andersen JN, Over H (2008) *J Phys Chem C* 112:9966
- Crihan D, Knapp M, Zweidinger S, Lundgren E, Weststrate CJ, Andersen JN, Seitsonen AP, Over H (2008) *Angew Chem Int Ed* 47:2131
- Amrute AP, Mondelli C, Schmidt T, Hauert R, Pérez-Ramírez J (2013) *ChemCatChem* 5:748
- Xiang G, Shi X, Wu Y, Zhuang J, Wang X (2012) *Sci Rep* 2:801
- Kondratenko EV, Amrute AP, Pohl M-M, Steinfeldt N, Mondelli C, Pérez-Ramírez J (2013) *Catal Sci Technol* 3:2555
- Zhang Q, Li R, Li Z, Li A, Wang S, Liang Z, Liao S, Li C (2016) *J Catal* 337:36
- Nguyen-Phan T-D, Luo S, Vovchok D, Llorca J, Sallis S, Kattel S, Xu W, Piper LFJ, Polyansky DE, Senanayake SD, Stacchiola DJ, Rodriguez JA (2016) *Phys Chem Chem Phys* 18:15972
- Balachadran U, Eror NG (1982) *J Solid State Chem* 42:276
- Shi J, Hui F, Yuan J, Yu Q, Mei S, Zhang Q, Li J, Wang W, Yang J, Lu J (2019) *Catalysts* 9:108
- Rochefort D, Dabo P, Guay D, Sherwood PMA (2003) *Electrochim Acta* 48:4245
- Zhao J, Xi W, Tu C, Dai Q, Wang X (2020) *Appl Catal B* 263:118237
- Madon RJ, O'Connell JP, Boudart M (1978) *AIChE J* 24:904
- Gonzo EE, Boudart M (1978) *J Catal* 52:462

Publisher's Note Springer Nature remains neutral with regard to jurisdictional claims in published maps and institutional affiliations.